JOURNAL OF MATERIALS SCIENCE 22 (1987) 3231–3239

Yttria–zirconia: effect of microstructure on conductivity

S. P. S. BADWAL, J. DRENNAN
CSIRO, Division of Materials Science and Technology, Normanby Road, Clayton, Victoria, Australia 3168

Complex impedance measurements and detailed analysis of the grain-boundary microstructure have been made on fully stabilized yttria–zirconia sintered bodies as a function of grain size. The prereacted yttria–zirconia powder used in this study was obtained from a commercial source. The powder has very high reactivity and starts sintering around 1200° C. The densification process is complete around 1350° C but the grain growth continues almost linearly with sintering temperature. The grain size variation obtained was between 1 and 30 μm. The grain-boundary resistivity when plotted against grain size showed an inflection in the vicinity of 1500° C sintering temperature. These results have been explained in terms of the grain-boundary microstructure changing with the sintering temperature. The thickness of the grain-boundary layer determined from impedance data and transmission electron micrographs are in reasonably good agreement. The activation energy for the grain-boundary resistivity was only slightly higher than that for the lattice resistivity.

1. Introduction

An important family of solid electrolytes is based on zirconia systems and these are now in common use in a variety of advanced technologies such as oxygen monitors and fuel cells. Polycrystalline materials are used in most of the studies and invariably in all the commercial applications because of the difficulty and expense associated with the fabrication of single crystals. Consequently, the grain boundaries play an important role in determining the conducting properties of polycrystalline materials. The fact that an interface exists between two adjacent grains gives rise to the formation of space charge layers due to constriction of the conducting pathways even in the absence of any impurities (intrinsic effect). The grain boundaries are, in the majority of cases, the sites of accumulation of less conducting secondary phases within the ceramic. These accumulations may be second-phase precipitation, increased concentration of dopant cation, contamination or sintering aid additions [1–4]. The physical and chemical nature of these phases, their structure and location – all of which may change with the sintering conditions – should have significant influence on the final conductivity of the material. Partial or complete blocking of the conducting species by the grain-boundary phases, in principle, would also lead to creation of space charge layers (extrinsic effects).

Impedance dispersion analysis has been used extensively in the examination and development of solid electrolytes after the initial report by Bauerle in 1969 [5]. The technique can effectively probe the lattice conductivity as well as the conductivity across interfaces which may include precipitates, grain boundaries or electrodes.

The aim of this work is to combine a detailed microstructural analyses of the grain boundaries with impedance dispersion technique with a view to examine the relationship between the microstructural development of a ceramic material and its conductivity. The system chosen was 10 mol % yttria-stabilized zirconia. The reason for this choice is, firstly, that the system has been studied extensively and the impedance characteristics well defined [6]. Secondly, the selection of this composition allows examination of an essentially single-phase material thus avoiding possible complications arising from the presence of precipitated phases. Finally, with the present technology of powder preparation it is now possible to obtain submicrometre high-purity prereacted powders [7]. This makes it possible, with judicious choice of sintering temperatures, to obtain homogeneous materials with a wide range of grain sizes for study of their impedance behaviour.

2. Experimental procedures

A fine-grain pre-reacted powder of 10 mol % Y_2O_3 + 90 mol % ZrO_2 (YSZ10V) was purchased from Viking Chemicals Ltd, Denmark. The supplied powder had a quoted purity level of 99.99% with silicon content around 0.001%. Because impurity levels, especially glassy phases have a marked effect on the electrical properties, the as-received powder was subjected to spectrographic analysis (inductively coupled plasma atomic emission spectroscopy, ICP; atomic absorption spectrometry, AAS; X-ray fluorescence, XRF; spark source mass spectrometry). The particle size distribution of the starting powder was measured using a Sedigraph ST500. For this, a small quantity of the powder was mixed with distilled water containing about 0.25 wt % of a deflocculant (Dispex A50) and then subjected to ultrasonic vibrations for 1 h.

0022–2461/87 $03.00 + .12

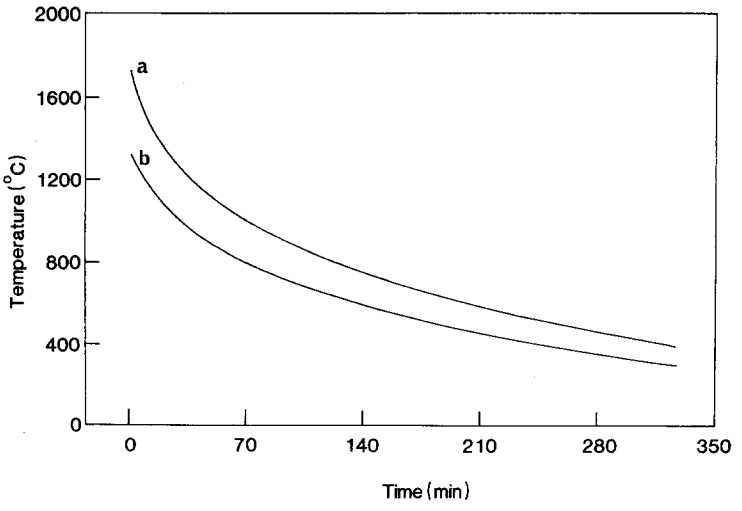

Figure 1 Cooling curves from sintering temperatures of (a) 1700° C, (b) 1300° C.

This powder, without any precalcination, was pressed into discs and sintered at various temperatures ranging from 900 to 1700° C in an air or argon atmosphere in conventional tube furnaces. The 1900° C specimens were sintered in a gas-fired furnace whilst embedded in the powder of the same composition to avoid impurity contamination. In the 900 to 1700° C temperature range the specimens were shielded from the furnace tube by a high-purity alumina work tube which was also used for control of the gas atmosphere. After sintering, the furnace was switched off and the cooling rate was controlled by the thermal inertia of the furnace. Fig. 1 shows cooling curves for specimens sintered at 1300° C and 1700° C. The cooling rate for specimens sintered in the gas-fired furnace at 1900° C was much higher. The sintered discs were about 9.2 to 9.4 mm in diameter and had a thickness of 2.5 to 3.0 mm.

Grain-size measurements were obtained from micrographs recorded from the polished and thermally etched specimens. Calculations of the grain sizes was based on a method described by Fullman [8]. For grain sizes less than 5 μm scanning electron microscopy was used. For this, mounted specimens were coated with a thin layer of carbon ($\sim$ 20 nm) to avoid charging problems. For grain sizes larger than 5 μm, optical microscopy provided the desired information. For detailed examination of the grain-boundary phases a number of samples were selected for analysis by transmission electron microscopy (TEM). Ion-beam thinned specimens were used for TEM work. Microscopes used were Hitachi S-450 LB for scanning electron work and Philips 420 for transmission electron work. Both microscopes were fitted with an energy dispersive X-ray analysis system. Table I gives nomenclature, sintering conditions, densities and average grain size for various specimens.

For conductivity measurements the discs were ground flat (320 grit silicon carbide powder), cleaned and painted with low impedance electrodes consisting of a mixture of platinum dioxide and a metal oxide such as fluorite structured $(U_{0.38}Sc_{0.62})O_{2\pm x}$. The data were collected with a Solatron model 1174 FRA over the frequency and temperature ranges of 1 Hz to 1 MHz and 375 to 600° C, respectively.

3. Results and discussion

3.1. Powder characterization

X-ray diffraction of the as-received powder showed the presence of a single phase with the fluorite structure. The mean particle size of the powder as determined by Sedigraph was $\sim$ 0.45 μm. Table II gives spectrographic analysis of the impurities. Although the silicon content was in the range quoted by the manufacturer, the total impurity level was found to be much higher.

3.2. Sintering behaviour and microstructure

The yttria–zirconia powder appears to have high reactivity and starts sintering at temperatures as low as

TABLE I Nomenclature, sintering conditions, density and grain sizes of various 10 mol % Y_2O_3 + 90 mol % ZrO_2 specimens

Nomenclature	Sintering conditions		Density, % theoretical	Average grain size (μm) ($\pm$ standard deviation)
	T ($\pm$ 10° C)	Time (h)		
YSZ10V10*	1000	48	56	–
YSZ10V11*	1100	36	61	–
YSZ10V12*	1200	24	71	0.5 $\pm$ 0.3
YSZ10V13†	1300	15	92	1.15 $\pm$ 0.08
YSZ10V14†	1400	15	97	6.1 $\pm$ 0.5
YSZ10V15†	1500	15	98	11.2 $\pm$ 1.1
YSZ10V16†	1600	15	98	15.1 $\pm$ 1.3
YSZ10V17†	1700	15	98	20.9 $\pm$ 1.1
YSZ10V19‡	1900	4	98	31.1 $\pm$ 3.1

* Specimens sintered in air.
† Specimens sintered in an argon atmosphere.
‡ Specimens sintered in a gas-fired furnace.

TABLE II Impurities in the starting powder

Element	Al	Ca	Mg	Fe	K	Na	S	P*	Ti*	Cr	V*	Cu*	Zn*	Mo*	Ni*	Pb*	Ce*	Si
Concentration ($\mu g\ g^{-1}$) ($\pm$ error)	< 50	270 ($\pm$ 50)	260 ($\pm$ 25)	60 ($\pm$ 20)	1100 ($\pm$ 60)	700 ($\pm$ 40)	1700 ($\pm$ 200)	30	30	10	10	10	30	5	5	50	5	20

* Accurate only to within a factor of 3.
Elements analysed by inductively coupled plasma atomic emission spectroscopy (ICP), Atomic absorption spectrometry, X-ray flourescence (S only) and spark source mass spectrometry.

1200° C. The density (as per cent theoretical) of the material after the 1200° C sintering is still low (71%) but the neck formation between particles was clearly observed with the scanning electron microscope. No clear evidence of this neck formation was observed for specimens sintered at 1100° C or below. This is further confirmed by the impedance data (Fig. 2) recorded for specimens sintered at 1000° C and 1200° C. The total resistivity of YSZ10V10 sample is dominated by the grain-boundary resistivity and it is about an order of magnitude higher compared with the YSZ10V12 specimen. Also in the latter sample the grain-boundary and lattice resistivity arcs are just beginning to separate.

The densification of the ceramic is almost complete around 1350° C but the grain growth continues linearily with temperature (Fig. 3) up to the maximum sintering temperature (1900° C) of this study. Fig. 4 shows grain size distribution for a specimen sintered at 1300° C. The average grain size was around 1 μm for these samples but it increased to 31 μm for specimens sintered at 1900° C. Fig. 5 shows micrographs recorded from two thermally etched specimens, one sintered at 1300° C and the other at 1700° C. The main observable differences between the two samples, apart from the large differences in their average grain size, is that the porosity in the 1300° C sintered specimen is all intergranular.

3.3. Impedance behaviour

The impedance spectra at 401° C for various specimens are shown in Fig. 6. The size of the lattice-resistivity arc (on the left) appears to remain constant but that of the grain-boundary arc (immediately to the right of lattice-resistivity arc) decreases monotonically with increase in the sintering temperature. Only a small part of the electrode arc (on the extreme right) is shown for clarity. In order to analyse the impedance data, a Cole–Cole distribution was considered to represent both the lattice (geometric) and grain-boundary relaxations. The separation of grain-boundary (R_{gb}) and lattice resistivity (R_l) contributions was made easier and more accurate when the data were represented by this model. The grain-boundary resistivity referred to in the text is the grain-boundary resistance normalized to 1 cm length and 1 cm^2 of the specimen surface area in contact with each electrode. The grain boundary surface area and the thickness have not been taken into account. In Fig. 7 the values of grain-boundary and lattice resistivities calculated at 401° C from impedance diagrams are plotted against the average grain size. The grain size has virtually no effect on the lattice resistivity. The grain-boundary resistivity, R_{gb}, on the other hand, decreases with increase in the grain size. The most striking feature of this diagram is the inflection point obvious in the grain-boundary resistivity against grain size curve between 1400 and 1600° C sintering temperatures. The validity of these results was confirmed by repeating impedance measurements on another set of specimens sintered at 1400, 1500 and 1600° C. In the absence of this effect, the normal behaviour is expected to be somewhat similar to that shown by the dotted line in Fig. 7 [1, 9].

Arrhenius plots for specimens sintered at different temperatures are shown in Fig. 8 for the total (symbols) and lattice (solid line) resistivities and in Fig. 9 for the

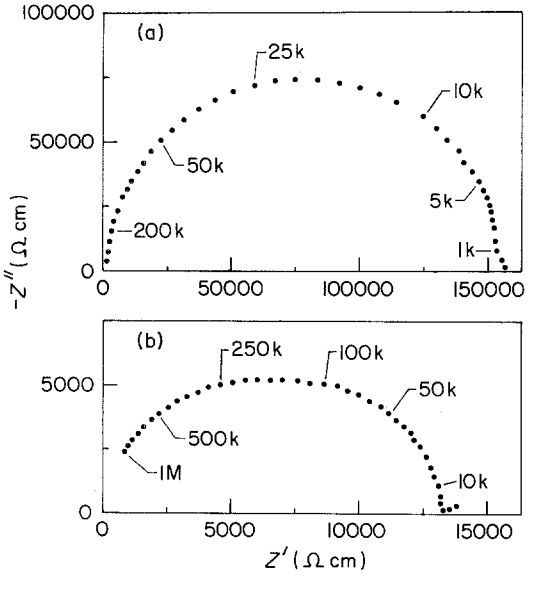

Figure 2 Impedance diagrams at 450° C for specimen sintered at (a) 1000° C, (b) 1200° C showing the onset of sintering.

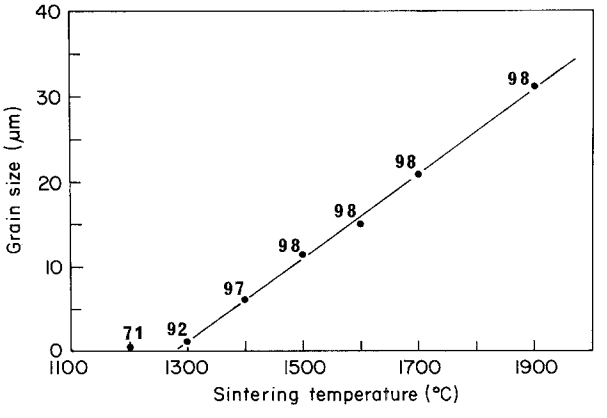

Figure 3 A plot of grain size against sintering temperature. The numbers on the curve indicate densities as a percentage of the theoretical.

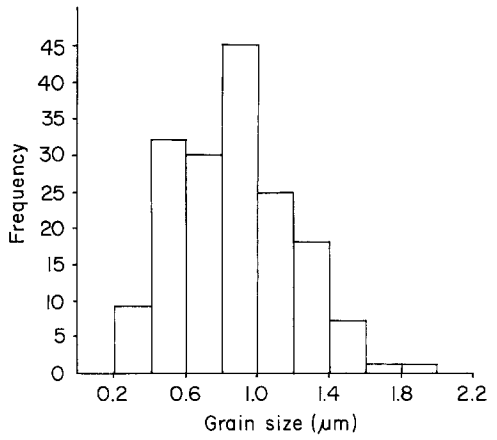

Figure 4 Grain size distribution for a specimen sintered at 1300° C.

grain-boundary resistivity. The activation energies calculated from $\sigma T = A \exp(-E/RT)$ relationship for the total, grain and lattice resistivities are given in Table III. The values for the activation energy of the grain-boundary resistivity is, on average, higher by about 5 to 6 kJ mol^{-1} than those for the lattice resistivity. These values are comparable with those reported earlier on 10 mol% Y_2O_3 + 90 mol% ZrO_2 in the low (350 to 500° C) temperature range when the same relationship (i.e. $\sigma T = A \exp(-E/RT)$) is used to calculate the activation energy [3].

3.4. Model

If we approximate the ceramic microstructure to consist of cubic grains of average cube length d and separated by the average grain boundary thickness δ_{gb}, the grain boundary capacitance, C_{gb} is given by

$$C_{gb}(A/L) = \varepsilon_0 \varepsilon_{gb} \frac{d}{\delta_{gb}} \quad (1)$$

TABLE III Activation energy for the total, grain-boundary and lattice resistivities over the temperature range 400 to 600° C

Specimen	Activation energy* (kJ mol^{-1})		
	Total	Grain-boundary	Lattice
YSZ10V10	117 ± 2	–	–
YSZ10V12	110 ± 2	–	–
YSZ10V13	114 ± 2	121 ± 3	110 ± 3
YSZ10V14	113 ± 2	118 ± 2	112 ± 2
YSZ10V15	114 ± 2	117 ± 2	113 ± 2
YSZ10V16	113 ± 2	113 ± 3	113 ± 2
YSZ10V17	113 ± 2	116 ± 4	112 ± 2
YSZ10V19	112 ± 2	116 ± 2	112 ± 2

*From $\sigma T = A \exp(-E/RT)$.

where A is the area of cross section of the specimen, L is the thickness of the disc, ε_0 and ε_{gb} are permittivities of free space and grain boundary material, respectively; the cube edge length, d, is given by $d = 0.806\, d_g$ where d_g is the average grain size determined for sphere-shaped grains [8]. In a real solid the values of both d and δ_{gb} are randomly distributed. However, for the sake of simplicity the average value for both quantities have been assumed. Wernicke [10], by computer simulations, has shown that such a brick-layer model approximation is reasonably descriptive of the ceramic microstructure.

According to the above relationship, C_{gb} should vary linearly with the grain size (or cube edge length) provided that there is no change in the thickness of the grain-boundary layer or the dielectric constant of the grain-boundary material as a result of differing sintering temperatures.

The plot of the grain-boundary capacitance C_{gb} (calculated from $\tau_{Cole-Cole} = R_{gb} C_{gb}$ relationship) against average cube edge length, d (Equation 1) is shown in Fig. 10 for our specimens at 401° C. There is

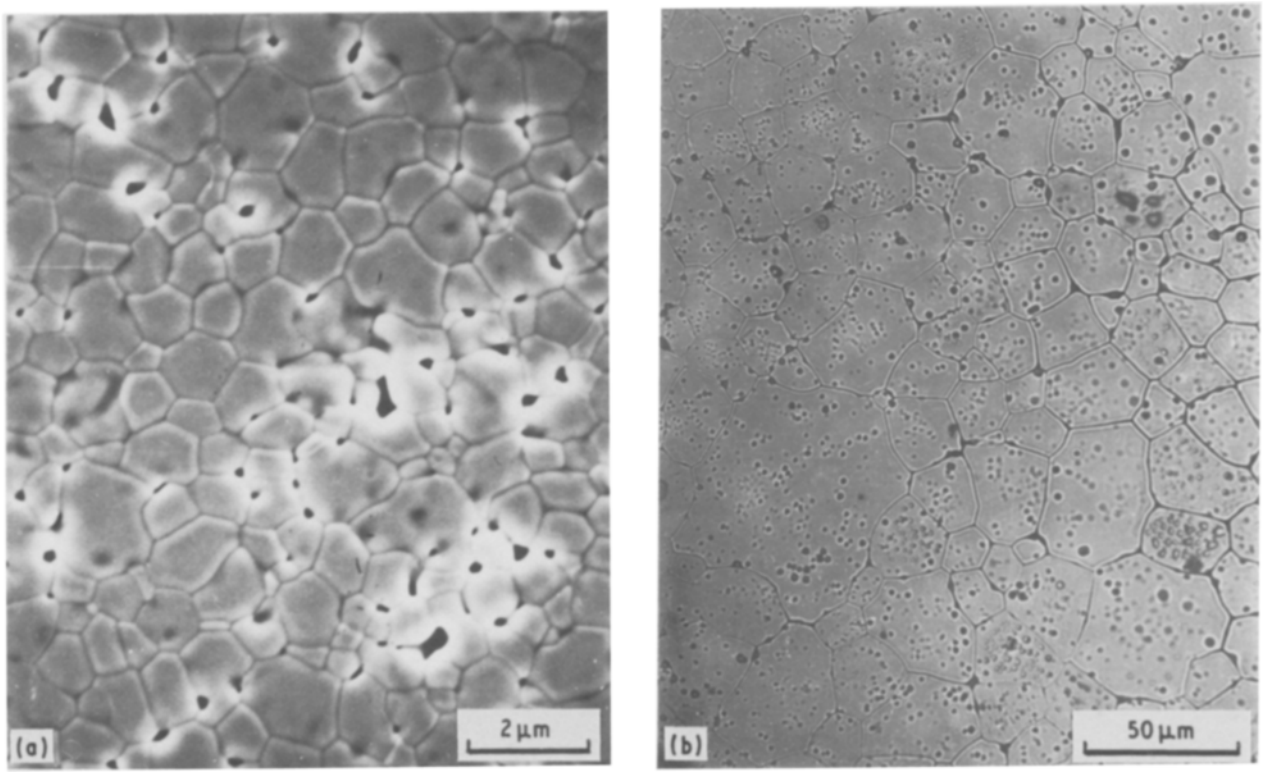

Figure 5 Micrographs of thermally etched specimens sintered at (a) 1300° C and (b) 1700° C.

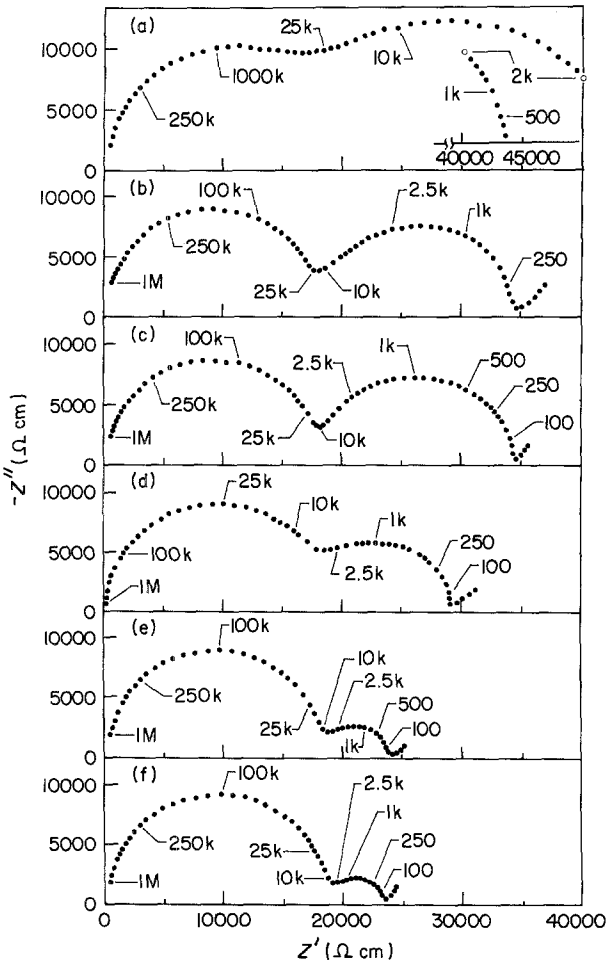

Figure 6 Complex impedance diagrams of various specimens at 401° C. Sintering temperature (a) 1300, (b) 1400, (c) 1500, (d) 1600, (e) 1700 and (f) 1900° C.

a marked change in the slope of the plot around 1500° C sintering temperature corresponding to the inflection observed in Fig. 7 for the R_{gb} against grain size curve. If the permittivity of the grain-boundary material remained constant this change in the slope is indicative of a decrease in the grain-boundary thickness for specimens sintered at temperatures above 1500° C. However, the composition, structure, physical nature (e.g. amorphous or glassy phase) and location of grain-boundary phase(s) may change for different sintering temperatures, thus creating uncertainty as to the validity of assuming a single permittivity value for the grain-boundary material. Considering a variation of the grain size is usually attained by sintering specimens at different temperatures, the change in the slope of C_{gb} against cube edge length (or grain size) curve therefore may not entirely be due to a change in the thickness of the grain-boundary layer.

Indeed transmission electron microscopy of specimens sintered at 1300, 1400 and 1600° C revealed the presence of impurities at grain boundaries. Specimens sintered at or below 1400° C were uniformly coated with an impurity phase at the interfaces between grains. The triple points were relatively free of any impurity phase as shown in Fig. 11 for a specimen sintered at 1300° C. Calculations based on the method of Clarke [11] using carefully oriented boundaries and a through focal series of micrographs suggested that this layer was in the vicinity of 0.8 ± 0.3 nm thick. Direct analytical information from boundaries only a few atoms thick is difficult to obtain; however, Fig. 12 shows the type of boundary phase observed in the through focal series displayed. More significantly, the nature of the accumulation changed progressively from being a uniformly dispersed film of several atoms thick at low sintering temperatures through to becoming relatively large isolated pockets along the boundaries and in triple points where the material has been sintered at higher temperatures (Fig. 11, 1300° C compared to 1600° C sintered specimens).

Energy dispersive X-ray analysis of the triple points observed in specimens sintered above 1500° C clearly revealed the presence of silicon. This is shown in Fig. 13 for a specimen sintered at 1600° C. In addition, the concentration of yttrium was much higher at such triple points compared with that in the bulk as shown in Fig. 13 and on the expanded scale in Fig. 14.

We offer the following explanation for the observed behaviour of specimens of the present study. For sintering temperatures around 1400° C or below the impurities are present at interfaces between grains. The nature of this phase, either amorphous or glassy, could not be established. Between 1400° C and 1500° C the impurity phase becomes less viscous or liquid, spreads out and at high temperatures is squeezed out into triple points. Therefore, as the sintering temperature increases above 1500° C the grain boundaries become cleaner. This unexpected dewetting

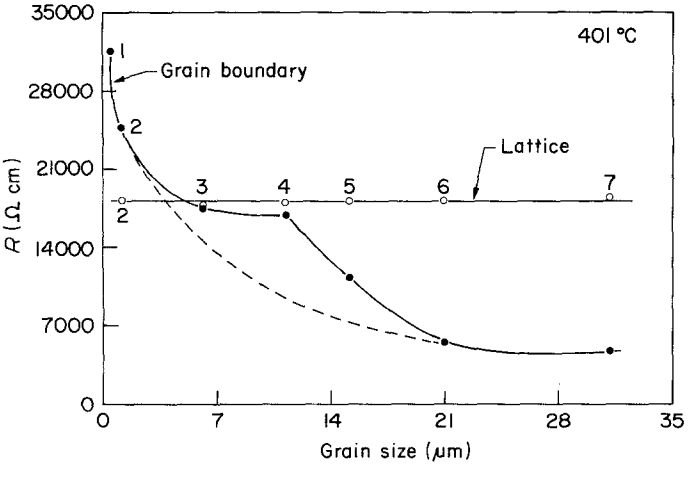

Figure 7 Plots of grain-boundary (R_{gb}) and lattice (R_l) resistivities against average grain size. The numbers on the curves indicate the sintering temperature. (1) 1200, (2) 1300, (3) 1400, (4) 1500, (5) 1600, (6) 1700, and (7) 1900° C.

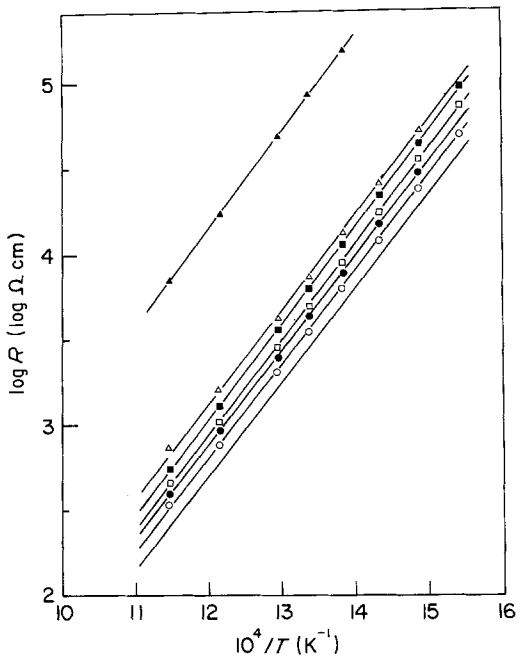

Figure 8 Arrhenius plots for the lattice (——) and total (symbols) resistivities of YSZ10V specimens. Sintering temperature: (▲) 1000; (△) 1200; (■) 1300; (□) 1400, 1500; (●) 1600; (○) 1700, 1900° C.

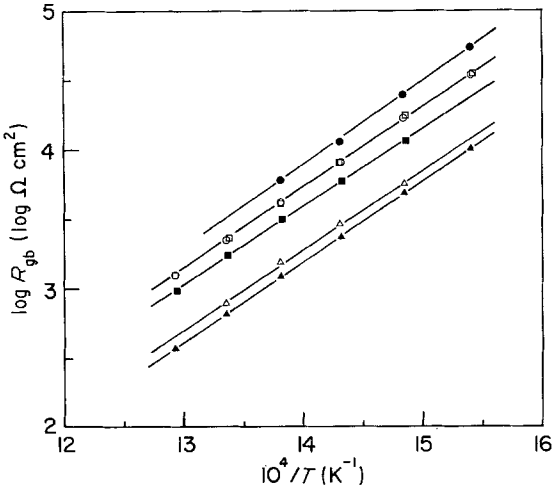

Figure 9 Arrhenius plots for the grain-boundary resistivities of YSZ10V specimens. Sintering temperature: (●) 1300, (□) 1400, (○) 1500, (■) 1600, (△) 1700, (▲) 1900° C.

of the grain boundaries at higher temperatures may have resulted from change in the chemical nature of the grain-boundary phase. Alternatively, it may have been caused by volatilization of the impurities. A third possible explanation is that dewetting may have occurred during cooling of specimens from the sintering temperature at which the grain-boundary phase was in the molten form.

In order to explain further the phenomena observed for the specimens of this study we have plotted the grain-boundary resistance per unit surface area of grain boundaries (R_{sp}) against grain-boundary density in Fig. 15. Such plots have been used before by Miyayama and Yangida [12] to explain intrinsic (pure space charge – in the absence of impurities) or extrinsic (impurity dominated) grain-boundary phenomena. If the grain-boundary resistivity was determined by intrinsic effects alone, the grain-boundary resistance per unit surface area of grain boundaries should not change with the grain size. Such a situation, however, rarely exists in polycrystalline materials. For the extrinsic grain-boundary phenomena if the total impurity content per unit volume of the ceramic and location of the impurity phases remained constant with the sintering temperature, the concentration of impurities per unit surface area of grain boundaries will increase with increase in the grain size or decrease in the grain boundary density. Therefore, for materials in which grain-boundary resistivity is impurity controlled, the grain-boundary resistance per unit surface area of the grain boundaries should increase with decrease in the grain-boundary density. This, in fact, is the case for our specimens up to the sintering temperature of 1500° C corresponding to the inflection points observed in the grain-boundary resistivity and grain-boundary capacitance against grain size curves. Above this temperature, as discussed earlier, when the grain-boundary phase starts dewetting the grain-boundaries and as they become more clean, R_{sp} starts decreasing with further decrease in the grain-boundary density. A slight increase for the 1900° C specimen may be associated with its significantly different cooling rate compared with other specimens and/or slight contamination in the gas-fired furnace.

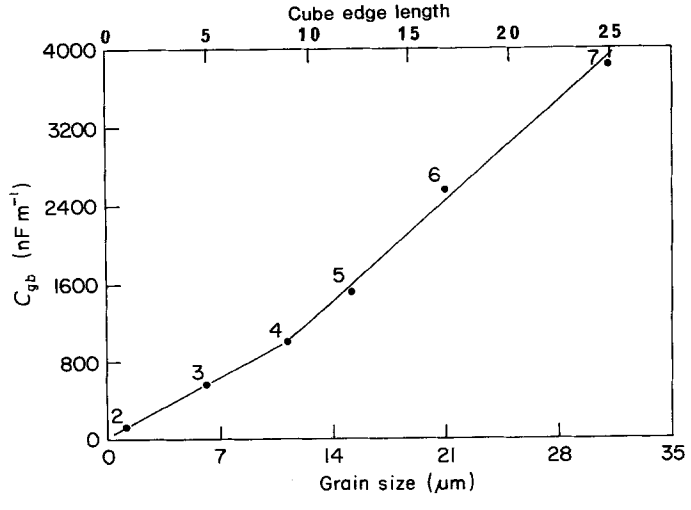

Figure 10 A plot of grain-boundary capacitance against average grain size (cube edge length) at 401° C. The numbers on the curve indicate sintering temperature as in Fig. 7.

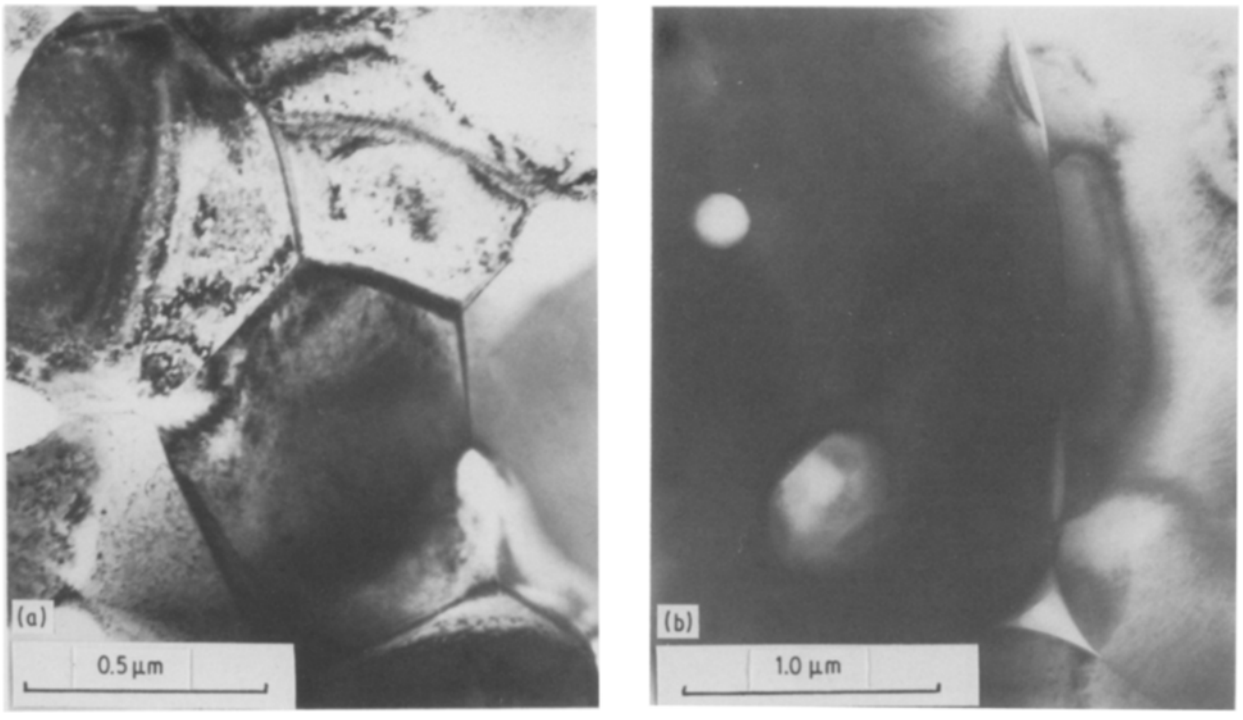

Figure 11 Transmission electron micrographs of YSZ10V specimens sintered at (a) 1300 and (b) 1600° C.

3.5. Grain-boundary thickness

We have also made an attempt to determine the grain-boundary thickness from the impedance data. Several authors have reported a value of between 22 and 25 for the permittivity of fully stabilized yttria–zirconia [13, 14]. If we assume these values for the grain-boundary material, as has been done by others [1], we calculate that the grain-boundary thickness is approximately 1.8 to 2.0 nm for specimens sintered below 1500° C. These values are somewhat higher than a value of 0.8 ± 0.3 nm determined from transmission electron micrographs recorded for a 1300° C sintered specimen. Two points should be made here: firstly, even if we had an ideal situation with the material free of impurities, to take the same value of permittivity for the grain boundaries as that for the bulk of the material is highly contentious; and secondly, we have shown that this material, as is the case

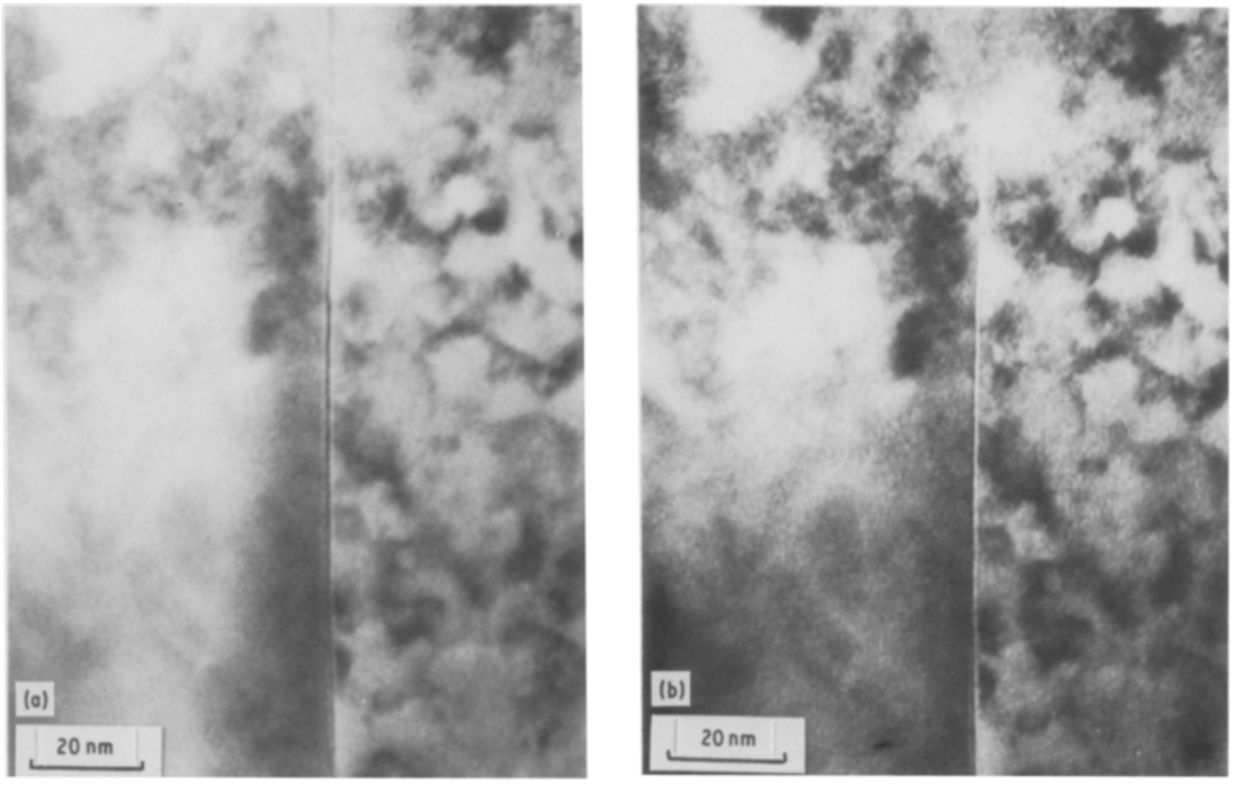

Figure 12 Transmission electron micrographs of a specimen sintered at 1300° C showing the behaviour of the grain-boundary phase as a function of through focus. (a) $+\Delta f$, (b) $-\Delta f$.

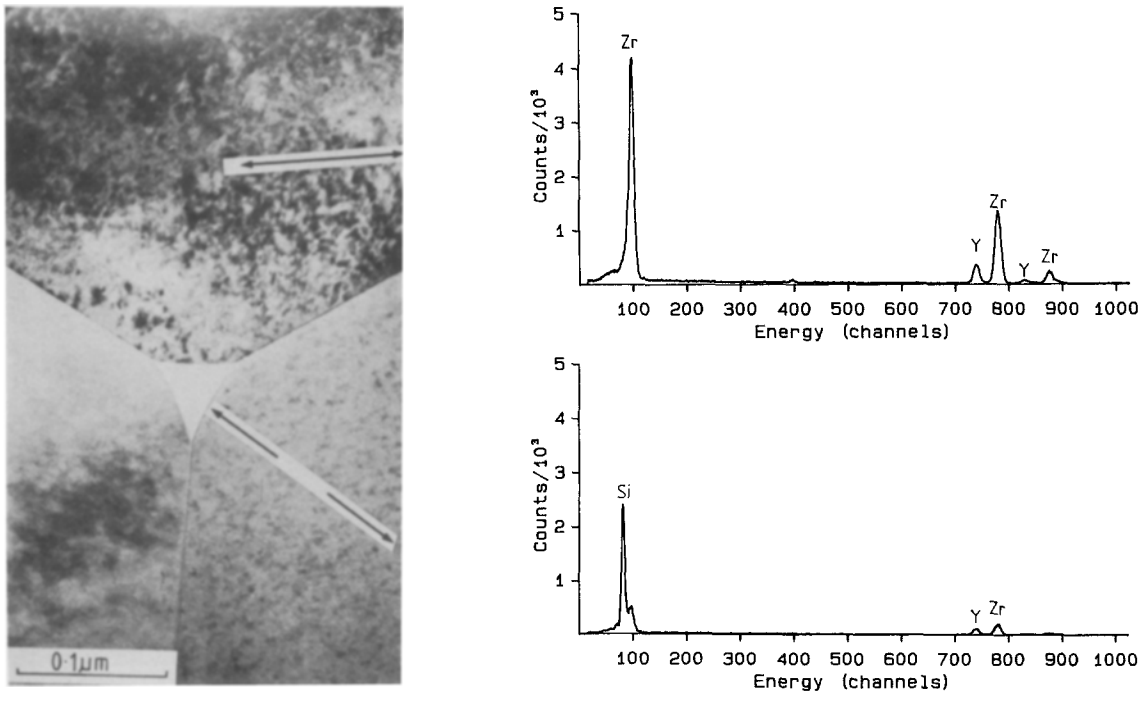

Figure 13 Energy dispersive X-ray analysis of a triple point and bulk of a grain along with a micrograph of the analysed area for a 1600° C sintered specimen, YSZ10V.

with all polycrystalline ceramics, contains impurities which tend to segregate at grain boundaries. To assume that this grain-boundary material will have the same permittivity as the bulk ceramics is not necessarily valid. For typical siliceous aluminious-type impurities the dielectric constant is much lower (6 to 9 [14]). The discrepancy between the δ_{gb} values determined from impedance data and transmission electron micrographs would be significantly reduced if a value of less than 22 to 25 for the permittivity of the grain-boundary material is used in calculating δ_{gb}.

4. Conclusions

The grain-boundary microstructure is easily influenced by the nature and amount of impurities, the sintering conditions and cooling rates. In order to understand the grain-boundary behaviour in solid electrolytes it is therefore essential to combine impedance dispersion measurements with the detailed analysis of the grain-boundary microstructure. Both these studies should be made on the same identical specimens, The grain-boundary impedance in the yttria–zirconia ceramics used in this study is impurity controlled.

Acknowledgements

The authors wish to thank K. Oatley and F. T. Ciacchi for their assistance with specimen preparation and grain-size analysis, and Mr L. S. Dale for spectrographic analysis of the yttria–zirconia powder.

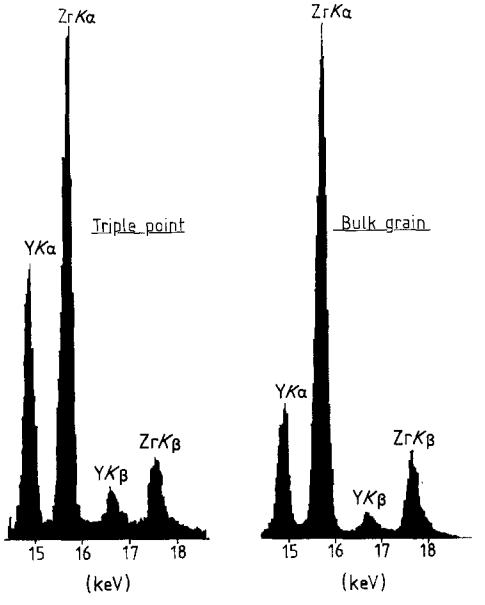

Figure 14 Energy dispersive X-ray analysis as in Fig. 13, for sample YSZ10V16. Expansion of right half of the spectrum.

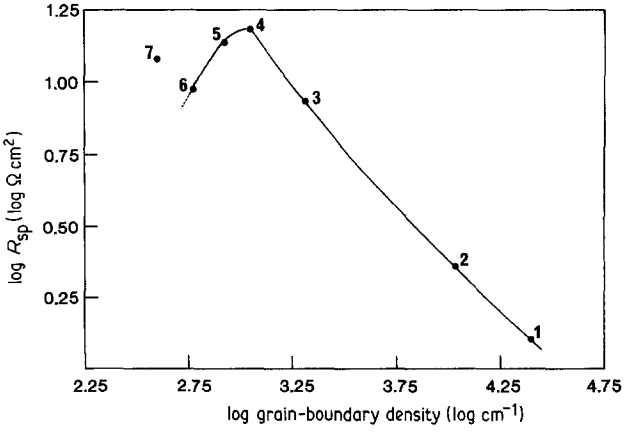

Figure 15 A plot of the grain-boundary resistance per unit surface area of the grain boundaries against grain-boundary density at 401° C. The numbers on the curves indicate sintering temperatures as in Figs 7 and 10.

References

1. M. J. VERKERK, B. J. MIDDLEHUIS and A. J. BURGGRAAF, *Solid State Ionics* **6** (1982) 159.
2. S. H. CHU and M. A. SEITZ, *J. Solid State Chem.* **23** (1978) 297.
3. S. P. S. BADWAL, *J. Mater. Sci.* **19** (1984) 1767.
4. A. J. A. WINNUBST, P. J. M. KROOT and A. J. BURGGRAAF, *J. Phys. Chem. Solids* **44** (1983) 955.
5. J. E. BAUERLE, *ibid.* **30** (1969) 2657.
6. M. KLEITZ, H. BERNARD, E. FERNANDEZ and E. SCHOULER, "Advances in Ceramics", Vol. 3, edited by A. H. Heuer and L. W. Hobbs (The American Ceramic Society, Columbus, Ohio, 1981) p. 310.
7. S. A. MARKLAND, Abst. D17, The Second International Conference on the Science and Technology of Zirconia, Stuttgart, West Germany, 21 to 23 June (1983). (Max-Planck-Institut für Metallforschung, Institut für Werkotoffwissenschaften, 1983)..
8. R. L. FULLMAN, *J. Metals AIME Trans.* **5** (1953) 447.
9. A. I. IOFFE, M. V. INOZEMTSEV. A. S. LIPILIN, M. V. PERFILEV and S. V. KARPACHOV, *Phys. Status Solidi (a)* **30** (1975) 87.
10. R. WERNICKE, "Advances in Ceramics", Vol. 1, edited by L. M. Levinson (The American Ceramic Society, Columbus, Ohio, 1981) p. 272.
11. D. R. CLARKE, *Ultramicroscopy* **4** (1979) 33.
12. M. MIYAYAMA and H. YANGIDA, *J. Am. Ceram. Soc.* **67** (1984) C194.
13. P. ABELARD and J. F. BAUMARD, *Phys. Rev. B* **26** (1982) 1005.
14. R. MORRELL, "Handbook of Properties of Technical and Engineering Ceramics", Part 1 (National Physics Laboratory, London, 1985).

Received 13 October 1986
and accepted 19 January 1987